147 (2023) 213329

Contents lists available at ScienceDirect

Biomaterials Advances

journal homepage: www.journals.elsevier.com/materials-science-and-engineering-c

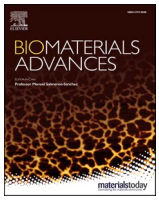

Bioprinting-associated pulsatile hydrostatic pressure elicits a mild proinflammatory response in epi- and endothelial cells

Ramin Nasehi [a], Jana Schieren [b], Caroline Grannemann [c], Alena L. Palkowitz [a], Aaron Babendreyer [c], Nicole Schwarz [b], Sanja Aveic [a], Andreas Ludwig [c], Rudolf E. Leube [b], Horst Fischer [a,*]

[a] Department of Dental Materials and Biomaterials Research, RWTH Aachen University Hospital, Pauwelsstraße 30, 52074 Aachen, Germany
[b] Institute of Molecular and Cellular Anatomy, RWTH Aachen University, Templergraben 55, 52062 Aachen, Germany
[c] Institute of Molecular Pharmacology, RWTH Aachen University Hospital, Pauwelsstraße 30, 52074 Aachen, Germany

ARTICLE INFO

Keywords:
Hydrostatic pressure
Bioprinting
Endothelial cells
Epithelial cells
Inflammatory response

ABSTRACT

During nozzle-based bioprinting, like inkjet and microextrusion, cells are subjected to hydrostatic pressure for up to several minutes. The modality of the bioprinting-related hydrostatic pressure is either constant or pulsatile depending on the technique. We hypothesized that the difference in the modality of hydrostatic pressure affects the biological response of the processed cells differently. To test this, we used a custom-made setup to apply either controlled constant or pulsatile hydrostatic pressure on endothelial and epithelial cells. Neither bioprinting procedure visibly altered the distribution of selected cytoskeletal filaments, cell-substrate adhesions, and cell-cell contacts in either cell type. In addition, pulsatile hydrostatic pressure led to an immediate increase of intracellular ATP in both cell types. However, the bioprinting-associated hydrostatic pressure triggered a pro-inflammatory response in only the endothelial cells, with an increase of interleukin 8 (*IL-8*) and a decrease of thrombomodulin (*THBD*) transcripts. These findings demonstrate that the settings adopted during nozzle-based bioprinting cause hydrostatic pressure that can trigger a pro-inflammatory response in different barrier-forming cell types. This response is cell-type and pressure-modality dependent. The immediate interaction of the printed cells with native tissue and the immune system in vivo might potentially trigger a cascade of events. Our findings, therefore, are of major relevance in particular for novel intra-operative, multicellular bioprinting approaches.

1. Introduction

Bioprinting is a powerful tool to arrange cells three-dimensionally (3D), which can enhance the physiologically favored spatial cell-cell and cell-matrix interaction during the subsequent maturation processes in vitro. Inkjet and micro-extrusion bioprinting are the most developed and widely used methods among bioprinting techniques [1–3]. During bioprinting, mechanical stresses due to the printing principle itself exert major influences on the cells. It is therefore important that those influences do not negatively affect the functionality of the processed cells allowing them to perform expected physiological activities.

The mechanical stresses occurring in the bioprinting process are hydrostatic pressure, shear stress, and extensional stress [4–7]. Hydrostatic pressure acts as the driving force to eject cell-laden hydrogel through the nozzle of the printer head. Shear stress results from friction force between the layers of the moving hydrogel through the nozzle. The highest shear stresses, however, occur near the stationary nozzle walls of the printer head. Extensional stress is imposed on the cells as they are passing through an abrupt change of the nozzle cross-section. There have been several studies investigating the effect of bioprinting-associated shear and extensional stresses on cells that show they are limiting factors in bioprinting since they affect cell viability by triggering apoptotic cell death [7,8].

In contrast to knowledge about the effects of shear and extensional stresses on cells, there still is not a complete picture of how the bioprinting-associated hydrostatic pressure influences cell behavior. It has been reported that very high hydrostatic pressure (above 200 MPa) causes programmed cell death [9]. Steward et al. [10] demonstrated that there is an interplay between cell-matrix interaction and

* Corresponding author.
E-mail address: hfischer@ukaachen.de (H. Fischer).

https://doi.org/10.1016/j.bioadv.2023.213329
Received 22 September 2022; Received in revised form 19 January 2023; Accepted 2 February 2023
Available online 8 February 2023

hydrostatic pressure that plays a role in the chondrogenic differentiation of mesenchymal stem cells. Maki et al. [11] showed that hydrostatic pressure triggers chromatin remodeling in chondrocytes. However, debates remain about the effect of low hydrostatic pressure, i.e., in the range of tens to hundreds of kPa, and of the depressurization rate on the cells in culture [12–15]. Nevertheless, strong evidence for the effect of low hydrostatic pressure on cells can be found in Solis et al.'s [16] study, which showed that a cyclic form of hydrostatic pressure, similar to that experienced by immune cells in the lung, can initiate an inflammatory response via the mechanically activated ion channel Piezo1. This underlines the importance of further study of the influence of low hydrostatic pressure on different cell types, as hydrostatic pressure is the basis of depositing cells using nozzle-based 3D bioprinting techniques.

In this study, the term bioprinting-associated hydrostatic pressure refers to hydrostatic pressure at the level relevant to the bioprinting applications that is imposed on cells when they are suspended in the medium. This clarification differentiates this study from those investigating the hydrostatic pressure effect on cells seeded on a substrate or those examining hydrostatic pressures outside of the bioprinting relevant range. Three process parameters are of importance when considering the bioprinting-associated hydrostatic pressure effect: the hydrostatic pressure amplitude, pulsation frequency, and total printing time. Moreover, with regard to the size of the printed structures, which is typically at the millimeter scale [17–21], the total printing time is in the range of minutes and in most cases no longer than 30 min. Based on these conditions [2,3,22,23], we compared two nozzle-based printing methods, i.e. microextrusion and inkjet bioprinting using mechanical microvalves, in terms of bioprinting-associated hydrostatic pressure at an amplitude of 1 bar, a pulsation frequency of 1 cycle/min, and a total time of 30 min. We hypothesized that, firstly, even at conservative parameter values, bioprinting-associated hydrostatic pressure is potent in triggering complex biological responses in the cells and, secondly, that the inkjet and micro-extrusion techniques differently trigger the biological cellular responses. The bioprinting-associated hydrostatic pressure effects were investigated on two representative cell types, primary human umbilical vein endothelial cells (HUVEC) and a human epidermal keratinocyte cell line (HaCaT). Each of the two cell types is physiologically accustomed to hydrostatic pressure due to their function as barrier cells.

2. Materials and methods

2.1. Microextrusion and inkjet bioprinting

The videos of bioprinting were made using a custom-built 3D-bioprinter. The printer comprised of microvalve-based (SMLD 300 G with 150 μm nozzle diameter, Fritz Gyger, Gwatt, Switzerland) as well as microextrusion print heads, mounted to a three-axis robotic system (Isel, Eichenzell, Germany). The printing pressure was set to 1.0 bar for both, microextrusion and inkjet bioprinting. Bioprinting was conducted at room temperature and using either alginate 1.5 % wt/v (for microextrusion technique) or alginate 3.0 % wt/v (for inkjet bioprinting). Alginate solutions were prepared by solving the respective amount of alginic acid sodium salt (Sigma-Aldrich, St. Louis, USA) overnight in deionized water (for the cell-free experiments) on the roller at room temperature. A network structure (2 × 2 mm) comprising five parallel lines in the x-direction intersecting with five other parallel lines in the y-direction was considered for bioprinting. Videos S1 and S2 were recorded using two separate cameras. The videos were used to clearly demonstrate that during inkjet bioprinting the biomaterial in the printer head reservoir is exposed to constant hydrostatic pressure (for minutes), while during microextrusion bioprinting, the biomaterial in the microextrusion printer head reservoir is exposed to pulsatile hydrostatic pressure due to frequent interruptions of the extrusion. The rest of the experiments in this work were conducted using cells suspended in their medium and using a custom-made pressure setup to exclusively study the effect of hydrostatic pressure on the cells. The same geometry, upstream hydrostatic pressure and printing speed were considered during both bioprinting techniques for videos S1 and S2.

2.2. Cell lines and primary cells

Immortalized human HaCaT keratinocytes were kindly provided by Prof. P. Boukamp [24]. The cells were cultured in DMEM (Dulbecco's Modified Eagle Medium) GlutaMax (Thermo Fisher Scientific, Waltham, MA, USA) supplemented with 10 % FCS and 1 % penicillin/streptomycin (PAN-Biotech, Aidenbach, Germany). Cells were passaged 2–3 days after reaching confluence as follows: the medium was removed from the flask and 5 ml of PBS (phosphate buffered saline) without $Ca^{2+/}Mg^{2+}$ was added to wash the residual medium. Then, cells were incubated with fresh PBS in 5 % CO_2 at 37 °C for 20 min. The PBS was carefully removed and 1 ml of 0.05 % Trypsin- 0.02 % EDTA (Ethylenediaminetetraacetic acid) solution (Pan Biotech) was added and incubated again at 37 °C for 10 min, after which 4 ml of culture medium were added to stop the Trypsin-EDTA reaction. The cell suspension was then transferred to a 15 ml conical tube and centrifuged at about 300 *g* for 3 min. The supernatant was carefully removed and cells were suspended in 5 ml of fresh, pre-warmed culture medium and seeded onto new T25 culture flasks with a split ratio of 1:5.

Primary HUVEC were isolated from umbilical cords provided by the Department of Gynecology and Perinatal Medicine (RWTH Aachen University Hospital) as approved by the local ethics committee of the Faculty of Medicine at RWTH Aachen University (EK 424/19). Briefly, the umbilical cords were rinsed in PBS for 5 min. In order to remove coagulated blood, the veins were flushed with PBS and then filled with collagenase solution (Collagenase Type I, 400 U/ml dissolved in Hank's Balanced Salt Solution with $CaCl_2$ and $MgCl_2$ both Gibco by Life Technologies, Carlsbad, USA) and closed with a clip at both ends. The umbilical cord was then placed on a petri dish and incubated for 30 min (37 °C and 5 % CO_2). The clips were then removed, and fresh PBS was used to flush the vein. The cell suspension was collected in a Falcon tube and centrifuged (300 *g* for 5 min; CT6EL, Hitachi Koki, Tokyo, Japan). The supernatant was removed from the tube and the remaining cell pellet was suspended with 10 ml medium (EBM-2 Basal Medium & EGM-2 SingleQuot Kit Supplement & Growth Factors, Lonza, Basel, Switzerland). The cells were transferred to gelatin-coated cell culture flasks (2 % gelatin from porcine skin, gel strength 300, Type A, Sigma-Aldrich, St. Louis, USA) and incubated at 37 °C and 5 % CO_2. The cells were cultured up to the fifth passage.

2.3. Pressure treatment

A custom-made pressure setup was used to stimulate cells with either constant and/or pulsatile hydrostatic pressure (Fig. S1). The setup was connected to a medical-clean high pressure air pipeline. A pressure regulator was used to set the proper upstream pressure. For pulsatile hydrostatic pressure, a solenoid valve controlled by an Arduino controller was used. The pressure regulator was set to 1 bar (additional to the atmospheric pressure of 101.3 kPa) and a pulsation frequency of 1 cycle/min for a total time of 30 min.

For each experiment and each repetition, 3 ml of cell suspension with a density of approximately $1{\cdot}10^6$ cells/ml was prepared and then divided into three 1.5 ml tubes, each one corresponding to one of the conditions. The tubes were transferred to 30 ml flat bottom tubes connected to the custom-made pressure setup (Fig. S1) and located in a heat block to be maintained at 37 °C throughout the experiment. While the control sample (Ctrl) was in contact with open air at atmospheric pressure, the constant pressure sample (Cons. P) was connected to medical air at constant 1 bar gauge pressure, and the pulsatile pressure sample (Puls. P) was connected to 1 bar gauge pressure medical air through a solenoid valve controlled by an Arduino controller stimulated by pulsatile hydrostatic pressure. After treatment with hydrostatic

pressure, the cell suspensions were collected for further analysis as described below.

2.4. Viability and cell size

Cell viability and size were measured using Countess II FL Automated Cell Counter (Thermo Fisher Scientific, Waltham, MA, USA). After treatment with hydrostatic pressure, 20 μl of each sample was collected and mixed 1:1 with Trypan Blue Stain solution 0.4 % (Invitrogen, Waltham, MA USA). Then, a 10 μl sample was added to a chamber slide and inserted into the Automated Cell Counter. Three samples per condition were used to measure the overall cell viability and sizes for each repetition.

2.5. RNA extraction and qRT-PCR

The cell suspension was centrifuged with 300 *g* at 4 °C for 5 min. The supernatant was removed and the cell plate was washed once with PBS. Then, buffer RLT (Qiagen, Hilden, Germany) was used for lysing the cells. Cell lysates were stored at −80 °C for later extraction of RNA. The RNA was extracted using RNeasy Kit (Qiagen, Hilden, Germany). RNA samples were quantified (NanoDrop, Peqlab, Erlangen, Germany) and identical amounts of mRNA within each data set were reversely transcribed using Prime-Script™ RT Reagent Kit (Takara Bio Europe, St-Germain-en-Laye, France) according to the manufacturer's protocol. The mRNA expression level of *IL-8*, *THBD*, *HES1,* and *HEY1* were measured by quantitative real-time PCR (qPCR) and normalized to the mRNA expression level of two reference genes. TATA-box binding Protein (*TBP*) and glucuronidase beta (*GUSB*) were chosen as the most stable reference genes based on the results from the geNorm algorithm included in the qbase+ software (biogazelle, Gent, Belgium). qPCR reactions were performed in duplicates using iTaq Universal SYBR Green Supermix (Bio-Rad, Feldkirchen, Germany) according to the manufacturer's instructions. The following primers were used with the primer annealing time given in brackets: *GUSB* (forward: TGCAGGTGATGGAAGAAGTG, reverse: TTGCTCACAAAGGTCACAGG; 60 °C), *HES1* (forward: GCACAGAAAGTCATCAAAGCC, reverse: GTATTAACGCCCTCGCAC; 59 °C), *HEY1* (forward: CCCAACTACATCTTCCCA, reverse: GTCAAAGTAACCTTTCCCTC; 59 °C), *IL-8* (forward: AAGACATACTCCAAACCTTTCC, reverse: ACTTCTCCACAACCCTCTG; 61 °C), *THBD* (forward: AGAGAAGAGACAAACACCT, reverse: TCCACAAGACCAGTAGAG; 57 °C), *TBP* (forward: GAGCCAAGAGTGAAGAACAGTC, reverse: GCTCCCCACCATATTCTGAATCT; 60 °C). All qPCR reactions were run on a CFX Connect Real-Time PCR Detection System (Bio-Rad, Feldkirchen, Germany) with the following protocol: 40 cycles of 10 s denaturation at 95 °C, followed by 10 s annealing at the indicated temperature and 15 s amplification at 72 °C. PCR efficiency was determined from the uncorrected RFU values using LinRegPCR version 2020.0. Relative quantification was performed with the CFX Maestro Software 1.1 (Bio-Rad).

2.6. Intracellular ATP

Total intracellular ATP was measured using an ATP Assay Kit (#ab83355, Abcam, Cambridge, UK). Briefly, $1{\cdot}10^6$ cells were harvested, washed with PBS, and suspended in 100 μl of ATP assay buffer. Cells were homogenized and centrifuged with 13,000 *g* at 4 °C for 5 min. The supernatants were collected, snap-frozen in liquid nitrogen, and stored at −80 °C for a later colorimetric assay procedures based on the manufacturer's protocol. Absorbance was measured at 570 nm using a spectrophotometer (SpectraMax M2/M2e, Molecular Devices, USA). The results are presented as the ratio between the treated and control samples.

2.7. Mitochondrial membrane potential

Tetraethylbenzimidazolylcarbocyanine iodide, JC-1 (#70014, Biotium, Fremont, CA, USA), a cationic dye that accumulates in energized mitochondria was added to the cell suspension at the end concentration of 5 μM. For control, the mitochondrial uncoupler FCCP (fluoro-carbonyl cyanide phenylhydrazone) (# sc-203,578, Santa Cruz, CA, USA) at the end concentration of 1 μM was added to the sample cell suspension. The red fluorescence in excitation (560 nm)/emission (590 nm) and green fluorescence excitation/emission (488 nm/530 nm) were measured using a spectrophotometer (SpectraMax M2/M2e, Molecular Devices, USA). Six flashes per reading at five points per well were considered. A background control was also provided for subtracting the background signal. The results are presented as the ratio of red to green fluorescence.

2.8. Immunocytochemistry and immunofluorescence microscopy analysis

The procedure for immunostaining was as follows: after treatment, cells were seeded on glass coverslips pre-coated with 2.5 μg/cm^2 human fibronectin (# 1918-FN, R&D Systems, Minneapolis, MN, USA), and incubated at 37 °C and 5 % CO_2. The seeding densities were about $6{\cdot}10^4$ cells/cm^2 and $1.5{\cdot}10^5$ cells/cm^2 for HUVEC and HaCaT, respectively. Cells were fixed either with 4 % PFA (Paraformaldehyde) or cold methanol depending on the selected cytoskeletal component to be stained. Cells were stored in PBS until further processing for no longer than 7 d. In the case of PFA fixation, a permeabilization step was added by incubating the samples with 0.1 % TritonX100 in PBS for 3 min, followed by three 5 min washing steps with PBS. For all samples, blocking was performed with 5 % (wt/v) bovine serum albumin (BSA, SERVA, Heidelberg, Germany) diluted in PBS for 30 min. Primary and secondary antibodies (described below) were diluted in 1 % (wt/v) BSA in 1xPBS. The samples were incubated with primary antibodies for 1 h at room temperature followed by a washing step in PBS and subsequent incubation with secondary antibodies for 1 h. After a final washing with PBS, samples were rinsed in distilled H_2O and mounted on glass slides with Mowiol (Carl Roth, Karlsruhe, Germany).

Guinea pig polyclonal antibodies against desmoplakin 1 and vimentin were from Progen Biotechnik (Heidelberg, Germany), rabbit polyclonal antibody against non-muscle myosin IIA from BioLegend (San Diego, CA, USA), murine monoclonal antibody against paxillin from BD Transduction Laboratories (South San Francisco, CA, USA), mouse polyclonal pan cytokeratin antibody cocktail from Thermo Fisher Scientific (Waltham, MA, USA) and VE-cadherin monoclonal antibody from Santa Cruz Biotechnology (Heidelberg, Germany). Alexa Fluor 488- and 555-conjugated secondary mouse, and 488-conjugated guinea pig antibodies as well as Alexa Fluor Plus 647-conjugated Phalloidin, were purchased from Invitrogen (Waltham, MA, USA). Alexa Fluor 488-conjugated secondary rabbit antibody was from Dianova (Hamburg, Germany). Nuclei were stained with Hoechst 33342 from Thermo Fisher Scientific (Waltham, MA, USA).

Microscopy recordings were performed using an Apotome.2 microscope (Carl Zeiss, Jena, Germany) and a 63×/1.40 N.A. DIC M27 oil immersion objective. Images were processed using ImageJ open-source software (National Institutes of Health, Bethesda, MD, USA). The images are presented as the maximum intensity projection after subtracting the background signal.

2.9. Quantification of stress-related proteins

Proteome Profiler Human Cell Stress Array Kit (R&D Systems, Minneapolis, MN, USA) was used for the quantification of stress-related proteins. Using this kit, 26 stress-related proteins were detected simultaneously (Fig. S2 and Table S1). The cell suspension was prepared at $2.0{\cdot}10^6$ cells/ml. After treatment with hydrostatic pressure cells were incubated at 37 °C at 5 % CO2 for 3 h. Then, cell lysates were prepared

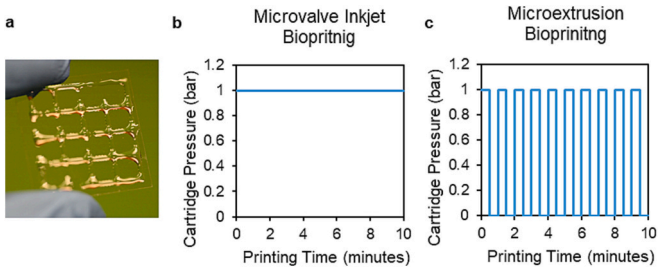

Fig. 1. Bioprinting-associated hydrostatic pressure modalities. (a) A sample network structure of alginate solution printed by inkjet bioprinting technique. (b) The hydrostatic pressure in the cartridge of the inkjet bioprinter during printing the pattern shown in a (video S1). (c) The hydrostatic pressure in the cartridge of the microextrusion bioprinter during printing a similar pattern shown in (a) (video S2).

and stored at −80 °C for later use. The assay was performed according to the manufacturer's recommendation. Proteins were quantified by measuring the pixel intensity of the individual spots normalized to the reference spots using ImageJ software.

2.10. Quantification of IL-8 protein

The ProQuantum Human IL-8 Immunoassay Kit (Invitrogen, Waltham, MA USA) was used to quantify the amount of IL-8 protein in the cell culture supernatant. After treatment of the HUVECs with hydrostatic pressure, they were incubated at 37 °C and 5 % CO_2. Cell culture supernatant was collected at two time points, 3 h and 6 h after treatment, and stored at −80 °C for later analysis. The assay was performed based on the manufacturer's protocol. Briefly, 5 μl of each sample were mixed with 5 μl of the antibody-conjugate mixture in a 96-well assay plate, sealed, and centrifuged at 3000 *g* for one minute. Then, the assay plate was incubated overnight at 4 °C. The day after, 40 μl of the qPCR reaction mixture was added to each assay well and mixed by pipetting up and down. The assay plate was sealed and centrifuged at 3000 *g* for one minute. The qPCR reaction was performed on Applied Biosystems 7900HT Fast Real-Time PCR System with the following setting: 45 cycles of 15 s denaturation at 95 °C, followed by 1 min annealing at 60 °C. A relative protein expression is calculated by 2(−delta CT) method and the results presented as a mean fold change for the pulsatile hydrostatic pressure condition (target) with respect to the control (reference) samples. Also, two different time points, 3 h and 6 h, were considered.

2.11. Statistical analysis

Data were obtained from at least three independent experiments. Statistical evaluation was performed on the raw data. The results are normalized to the control samples and presented as mean ± SD. One-way ANOVA followed by Dunnett's Multiple Comparison (GraphPad Prism 7 software) was used. The differences were considered significant at $*p < 0.05$, $**p < 0.01$.

3. Results

3.1. The bioprinting-associated hydrostatic pressure modalities

The two well-established nozzle-based bioprinting techniques, inkjet, and micro-extrusion, differ in terms of the modality of bioprinting-associated hydrostatic pressure. Video S1 and video S2 show the bioprinting process during printing the simple network structure presented in Fig. 1 (a). Using the inkjet bioprinting method, flow is controlled by the cyclic opening and closing of a microvalve at the tip of the nozzle (when using a mechanical microvalve), but the cell-laden hydrogel inside the printer head cartridge is exposed to constant hydrostatic pressure (video S1 and Fig. 1(b)). In contrast, when using the microextrusion

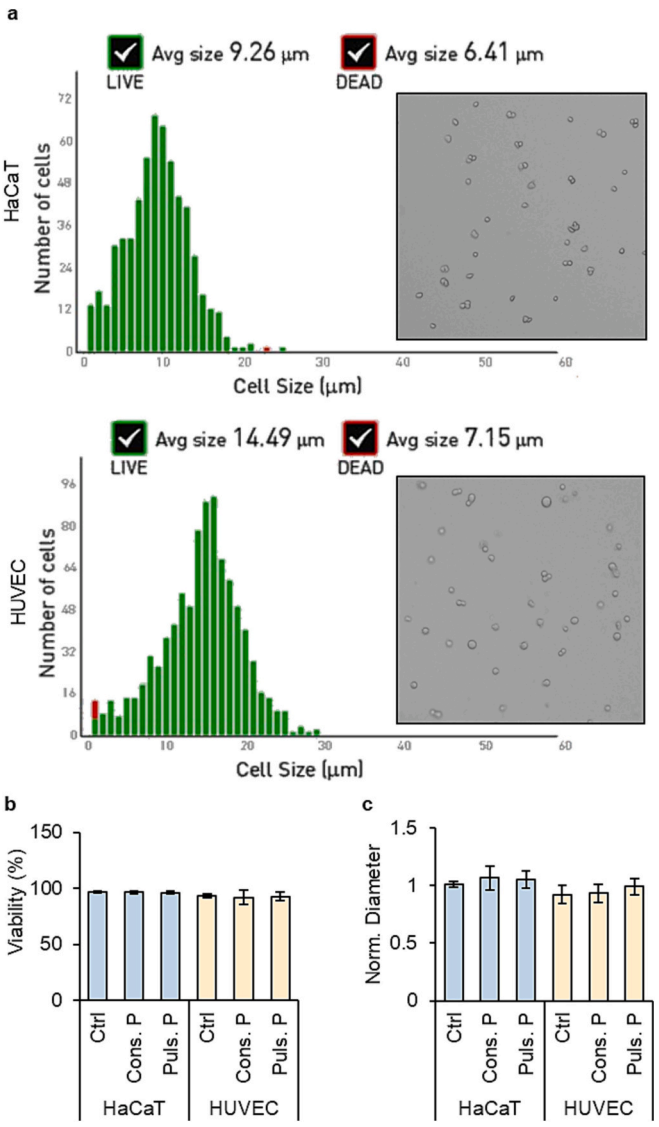

Fig. 2. (a) Representative sample results from Countess II FL Automated Cell Counter for HaCaT cell line and primary HUVEC. The cell counter automatically gives the viability results together with cell size distribution. Note that the inserted images of cells are part of the whole field of view; therefore, the total number of cells in the graphs does not match the total number of cells in the inserted images. (b) Cell viability and (c) cellular size immediately after treatment with hydrostatic pressure. Control (Ctrl) refers to the sample at atmospheric pressure, Cons. P refers to the samples treated with constant hydrostatic pressure and Puls. P refers to those treated with pulsatile hydrostatic pressure. No statistically significant differences were found between the different groups. Data is normalized to pretreatment values and presented as the mean ± SD (n = 4).

bioprinting technique, flow is controlled by the upstream pressure itself. Thus, the cell-laden hydrogel flow is regulated by cyclically switching the driving pressure on and off, meaning the processed cells are exposed to pulsatile hydrostatic pressure (video S2 and Fig. 1(c)). This experiment was performed using an alginate solution just to clarify the difference in hydrostatic pressure modalities between these two techniques. In the rest of this work, cells were suspended in their normal culture medium to exclude any cell-matrix interactions and only study the effect of hydrostatic pressure itself on the cells.

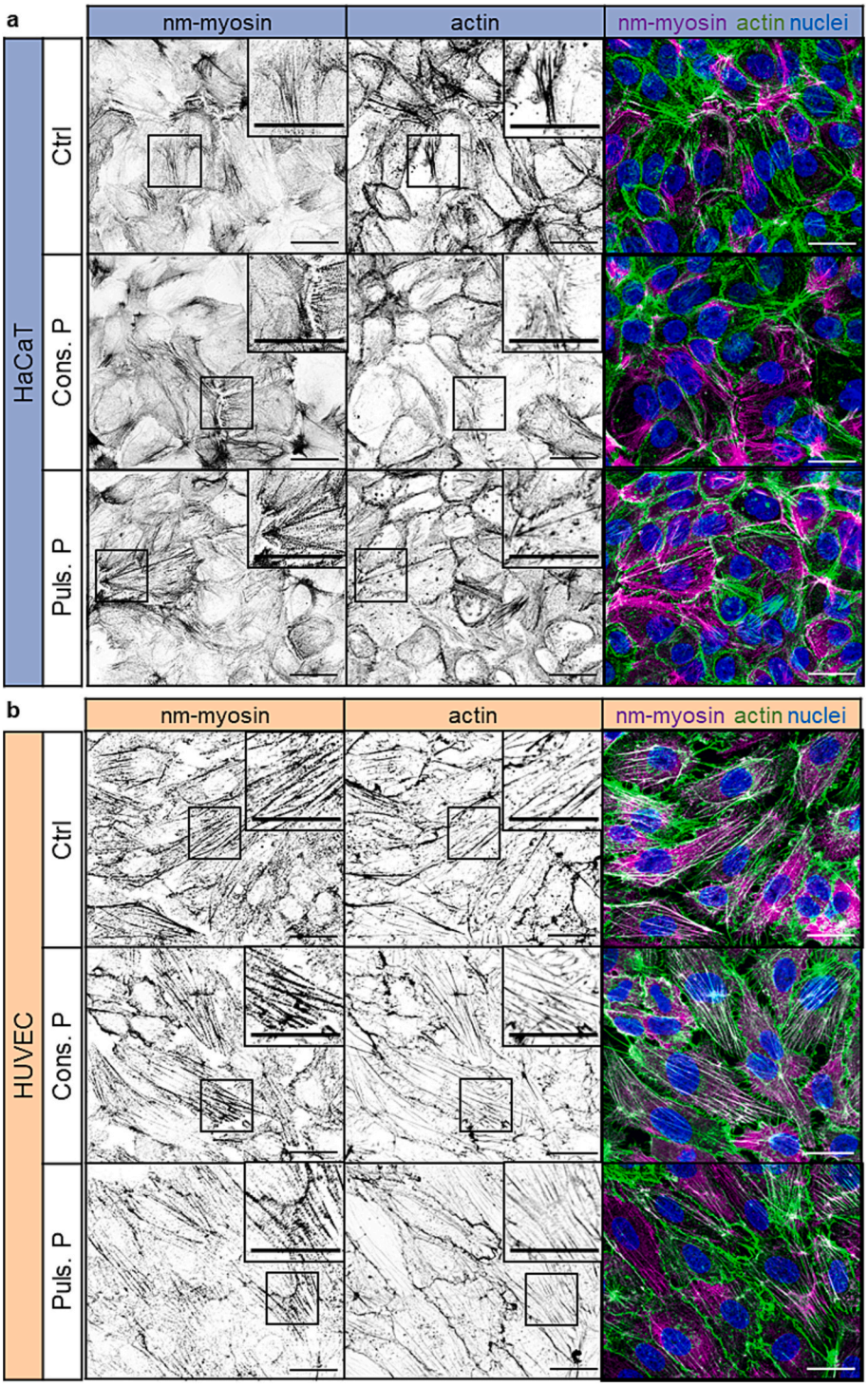

Fig. 3. Non-muscle myosin and actin filaments. (a) HaCaT cell line: The structure of the control group actin filaments and non-muscle myosin (nm-myosin) is compared with samples treated with constant pressure (second row) and pulsatile pressure (third row). (b) HUVEC: The structure of actin filaments and nm-myosin of the control group is compared with samples treated with constant pressure (second row) and pulsatile pressure (third row). The first and the second columns show the corresponding cellular components in a single channel in grayscale; the third column shows the merged image in color. Scale bars: 25 μm.

3.2. Cell viability and sizes

To eliminate the effect of bioprinting-associated shear stress and exclusively study the bioprinting-associated hydrostatic pressure, a custom-made pressure setup was used to stimulate cells with constant or pulsatile hydrostatic pressure (Fig. S1). This setup enabled us to simultaneously treat six individual samples, three with constant and three with pulsatile pressure. HUVEC and HaCaT cells were chosen for the experiments since each of the two cell types is physiologically accustomed to hydrostatic pressure due to their function as barrier cells. Fig. 2 (a) shows the representative results obtained by an automated cell counter. The results include cell viability and cell size distribution. The normalized viability of the cells immediately after treatment with gauge hydrostatic pressure of 1 bar for 30 min is shown in Fig. 2(b). Neither hydrostatic pressure modality caused any cell damage that led to the immediate death of cells in HaCaT or HUVEC.

Cells in suspension appeared almost spherical. Fig. 2(c) presents the normalized average diameter of cells immediately after pressurization. No significant change in the diameter of cells is observed.

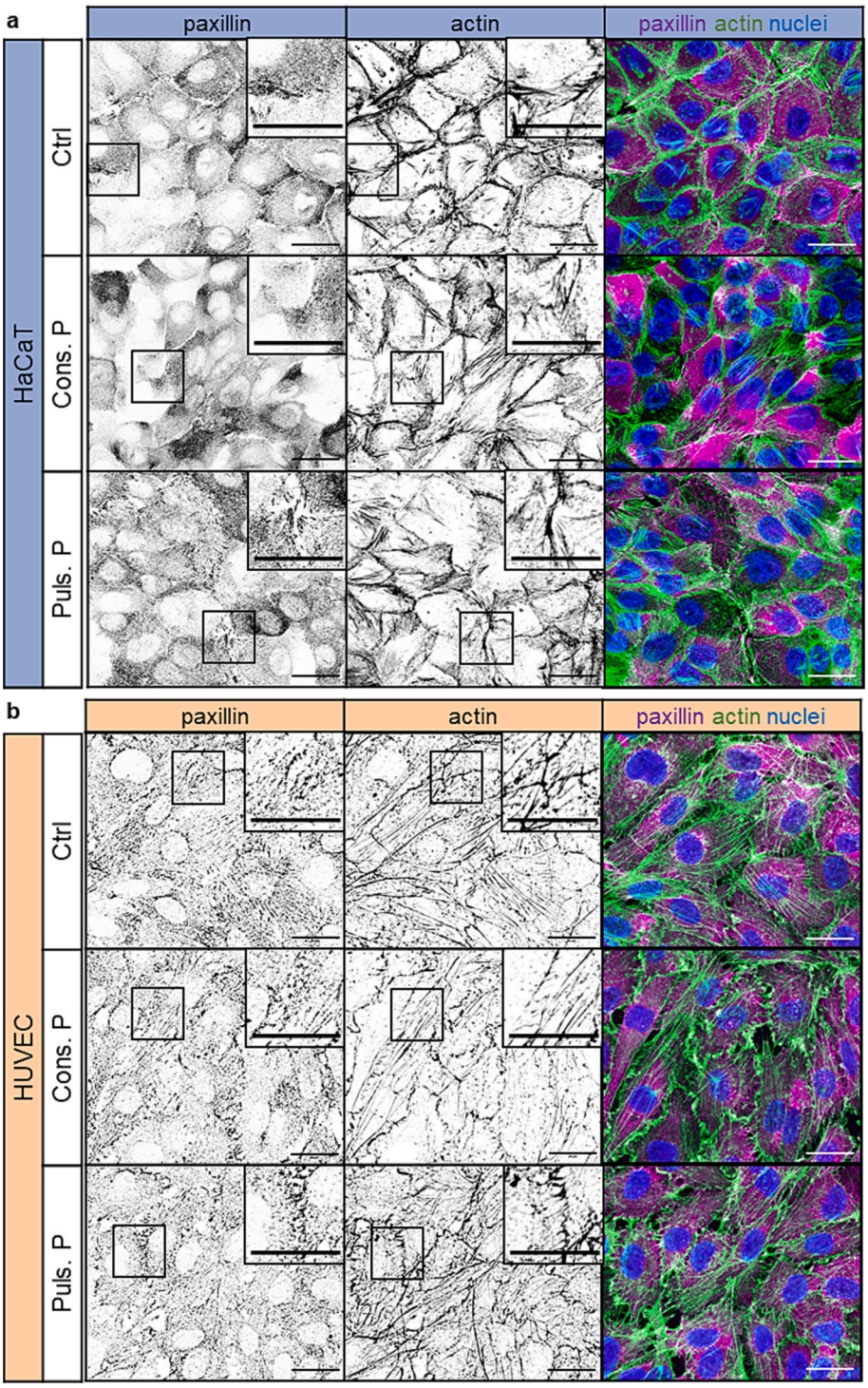

Fig. 4. Cell-substrate contacts and actin filaments. (a) HaCaT cell line: The structure of focal adhesions (paxillin) and actin of the control group is compared with samples treated with constant pressure (second row) and with pulsatile pressure (third row). (b) HUVEC: The structure of focal adhesion (paxillin) and actin of the control group is compared with samples treated with constant pressure (second row) and with pulsatile pressure (third row). The first and the second columns show the corresponding cellular components in a single channel in grayscale; the third column shows the merged image in color. Scale bars: 25 μm.

3.3. Cell cytoskeleton

One of the basic characteristics of epithelial and endothelial cells is their ability to form a confluent monolayer that can serve as a physical barrier. To determine whether bioprinting-associated hydrostatic pressure disrupts this functionality by changing the structure of the cytoskeleton, we used immunocytochemistry to visualize selected cytoskeletal structures. To do so, cell suspensions were subjected to hydrostatic pressure and seeded on fibronectin-coated coverslips. After 24 h, cells were fixed and stained for specific cytoskeletal components.

3.3.1. Non-muscle myosin and actin filaments

Non-muscle myosin is associated with the cell cytoskeleton and plays role in cell protrusion, adhesion and polarity through ATP-dependent motor activity and contractile properties [25,26]. HaCaT cells and HUVEC were co-immunostained for actin filaments and non-muscle myosin 24 h after treatment with hydrostatic pressure. Fig. 3(a) and (b) show separately in grayscale these two protein structures and in color (third column) the merged images for HaCaT cells and HUVEC, respectively. Our visually structural comparison between Ctrl and treated samples, i.e., Cons. P and Puls. P, do not reveal any visible disruption/change in the structure of either actin or non-muscle myosin.

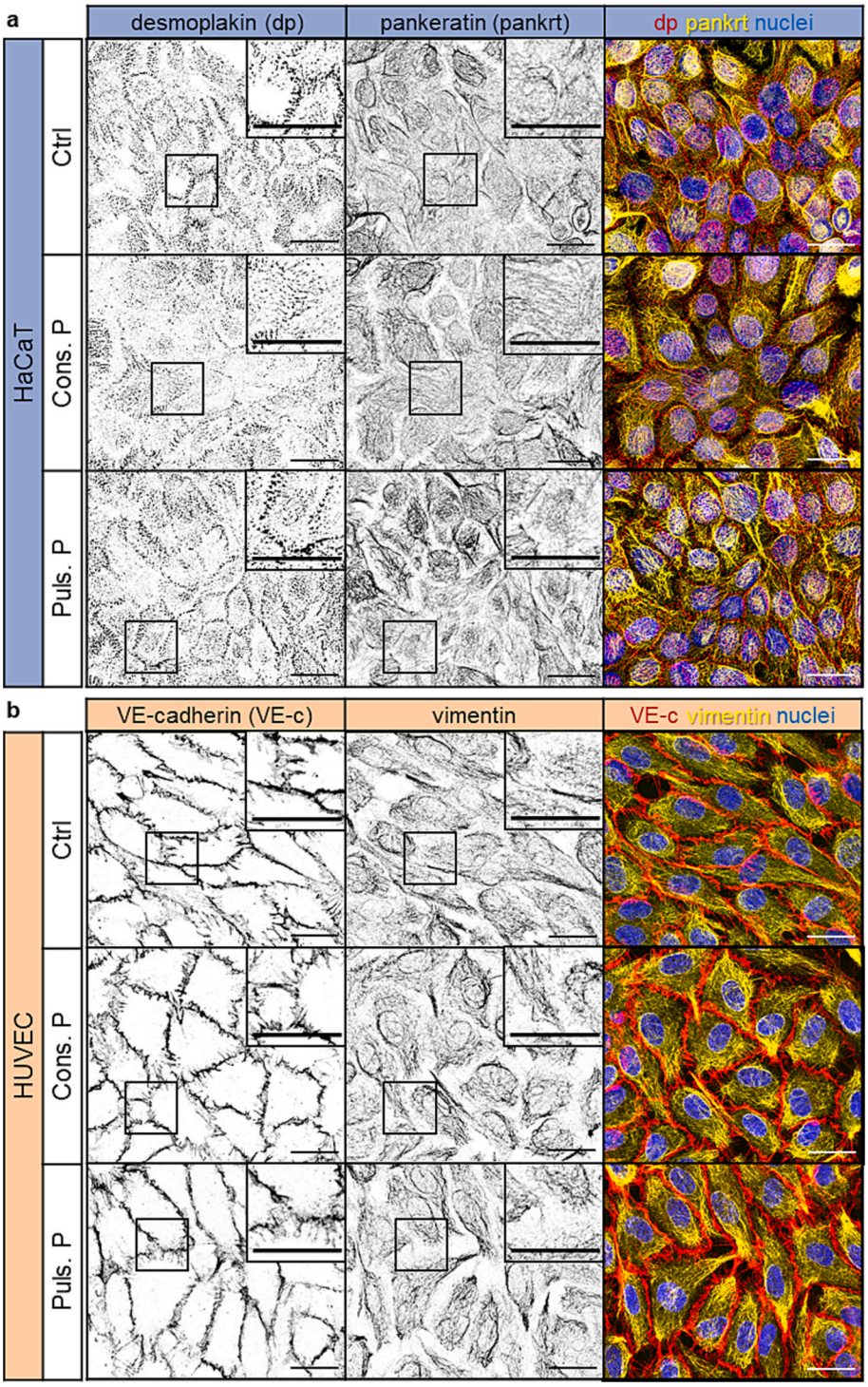

Fig. 5. Cell-cell contacts and intermediate filaments. (a) HaCaT cell line: The structure of cell-cell contacts (desmoplakin) and intermediate filaments (pankeratin) of the control group is compared with samples treated with constant pressure (second row) and with pulsatile pressure (third row). (b) HUVEC: The structure of cell-cell contacts (VE-cadherin) and intermediate filaments (vimentin) of the control group is compared with samples treated with constant pressure (second row) and with pulsatile pressure (third row). The first and the second columns show the corresponding cellular components in single channel in grayscale; the third column shows the merged image in color. Scale bars: 25 μm.

3.3.2. Cell-substrate contacts via focal adhesion

Paxillin is a focal adhesion-associated protein that binds to other proteins involved in actin cytoskeletal organization and plays a role in several signaling pathways [27,28]. The co-localization of actin and paxillin shows special distribution/organization of cell-matrix interaction via focal adhesions. Fig. 4(a) and (b) represent the immunofluorescence images of HaCaT and HUVEC, respectively, co-stained with actin and paxillin. Based on our results, neither actin nor focal adhesions containing paxillin showed any visible differences in their size, distribution, or structure comparing control with treated samples for both cell types.

3.3.3. Cell-cell contacts and intermediate filaments

The proteins on the surface of the cells enable them to interact with each other and mediate cell-cell contact. Stable cell-cell junctions are required for the organization of cells in tissues. Desmosomes are critically important to the functioning of epithelial cells as a physical barrier [29]. Fig. 5(a) presents the immunofluorescence images of HaCaT cells stained for desmoplakin and keratins. The formation of desmosomes at the boundaries of cells where they attach to each other is clearly evident for all treated and control samples. We were not able to distinguish any structural differences between control and treated samples in either the keratin network or desmosome organization/distribution.

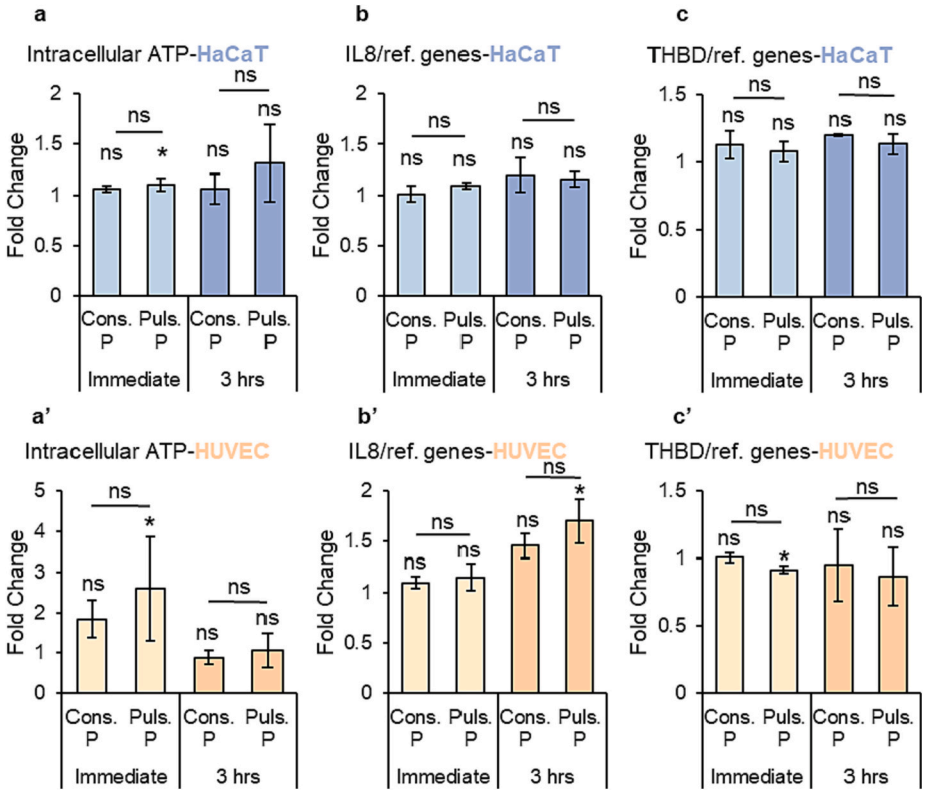

Fig. 6. Pro-inflammatory factors. Pulsatile hydrostatic pressure immediately raises the intracellular ATP of HaCaT cell line (a) and primary HUVEC (a'). While both modalities of hydrostatic pressure do not affect *IL-8* mRNA expression level of HaCaT cells (b), in the pulsatile form it increases *IL-8* mRNA expression of HUVEC after 3 h. For HaCaT cells, the expression level of thrombomodulin (*THBD*) remains the same for control and treated samples (c). For HUVEC, pulsatile hydrostatic pressure immediately decreases the *THBD* mRNA expression (c'). All data are normalized to values corresponding to Ctrl sample (corresponding to the value = 1) and presented as fold change. The statistical analysis was performed on raw data ($n \geq 3$ and $^*p < 0.05$).

Vascular endothelial (VE)-cadherin is an endothelial-specific adhesion molecule that is crucial for the maintenance of endothelial cell contacts and for the control of vascular permeability [30]. Vimentin is the type III intermediate filament protein that plays role in cell adhesion, migration, and angiogenesis [31]. HUVEC were stained for VE-cadherin and vimentin (Fig. 5(b)). The immunofluorescence images show that hydrostatic pressure, both pulsatile and constant, neither impairs the VE-cadherin-containing cell-cell contacts of HUVEC nor the structure and distribution of vimentin.

3.4. Cellular pro-inflammatory response

Adenosine triphosphate (ATP) provides energy for the cell and is involved in many cellular processes, including signaling [32]. Fig. 6(a) and (a') show that the printing-associated hydrostatic pressure immediately increased the intracellular ATP of both HaCaT cells and HUVEC. The increase in intracellular ATP was only significant for the pulsatile pressure modality, i.e., representing the micro-extrusion method, and was more pronounced in HUVEC than in HaCaT cells (HaCaT: 10 % increase in the mean value; HUVEC: 158 % increase in the mean value). The level of ATP returned to the baseline 3 h after the treatment, indicating that the effect was temporary.

Many of the cells, including endothelial and epithelial cells, produce interleukin 8 (IL-8) [33]. This pro-inflammatory factor has a chemotaxis effect and the potential in promoting angiogenesis [34,35]. The qPCR results showed that the effect of printing-associated hydrostatic pressure on the mRNA expression of *IL-8* depends on cell type and pressure modality (Fig. 6(b) and (b')). While the mRNA expression of *IL-8* was not affected by hydrostatic pressure for HaCaT cells, it was increased for HUVEC treated with pulsatile pressure. The level of this pro-inflammatory cytokine was significantly higher than the baseline 3 h after pressurization. Thrombomodulin (*THBD*) is a transmembrane molecule able to bind thrombin. When activated on the surface of the endothelium it acts as an anticoagulant and anti-inflammatory factor [36,37]. Our results (Fig. 6(c')) further indicated that pulsatile hydrostatic pressure slightly decreases the *THBD* gene expression of HUVEC, pointing toward an antithrombotic response activity. However, this is a temporary event and the *THBD* mRNA level returns to its baseline, as determined by control samples, after 3 h. Hydrostatic pressure in constant modality did not affect *THBD* transcriptional level. Moreover, the response to the pressure is cell type dependent because the expression of *THBD* was not affected in HaCaT cells in either of the hydrostatic pressure modalities (Fig. 6(c)).

The cell stress proteome profiling array was used to evaluate a spectrum of cell stress-related proteins after treatment with hydrostatic pressure. Using Proteome Profiler Human Cell Stress Array Kit, 26 human cell stress-related proteins can be detected simultaneously. The experiment was performed for two donors of primary HUVECs, and two conditions: control and pulsatile pressure. In Fig. 7(a) the dot blots are presented. The evaluation of the intensity of the pixels is presented in Fig. 7(b) and (c). No significant and consistent change in any of the stress-related proteins was detected for the analyzed donors.

The ProQuantum Human IL-8 Immunoassay Kit was used to quantify the IL-8 protein of primary HUVECs after treatment with pulsatile hydrostatic pressure. The change of IL-8 protein level was not significant 3 h after treatment (1.69 ± 0.16 fold change) with respect to control samples (1.00 ± 0.28 fold change). However, the measurement revealed a 3.18 ± 1.27 statistically significant fold increase in IL-8 protein 6 h after treatment with respect to the same control samples (Fig. 8).

3.5. Mitochondria and Piezo1 activity

Mitochondria are mechanoresponsive organelles and one of the major sources of ATP production within a cell [38,39]. Since the intracellular ATP is increased in response to pulsatile hydrostatic pressure for both cell types, it was of interest to see whether mitochondria are affected by hydrostatic pressure. The mitochondrial membrane potential was measured by using JC-1 cationic dye immediately and 3 h after the pressure treatment. The results (Fig. 9(a) and (a') for HaCaT and HUVEC, respectively) are represented as the ratio of red (high

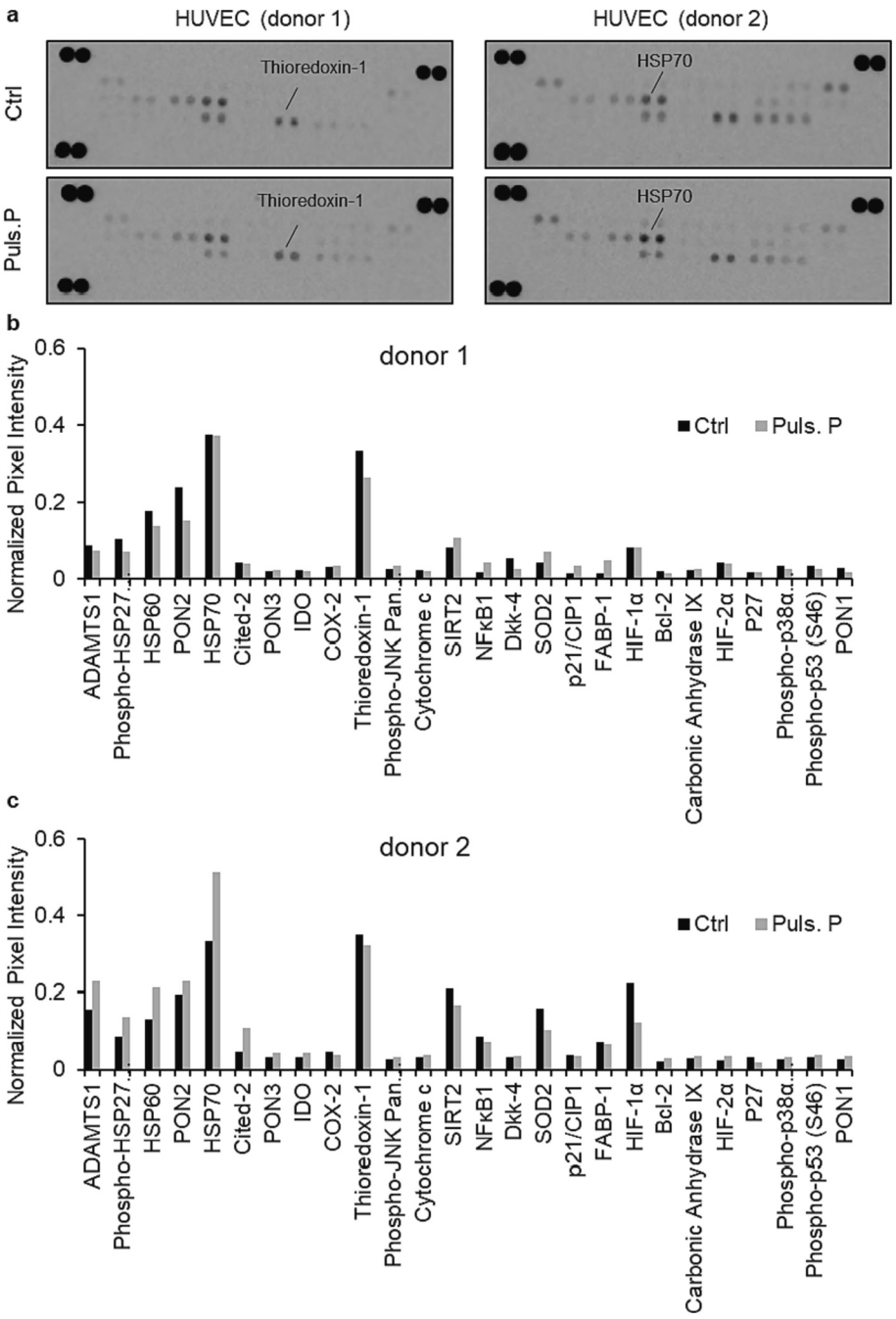

Fig. 7. Cell stress proteome profiling array. The proteome dot blots of two primary HUVECs donors are presented in (a) for two experimental conditions of control (Ctrl) and pulsatile pressure (Puls. P). The evaluation of pixel intensities for each of the 26 stress-related proteins are presented in (b) and (c). Thioredoxin-1 was slightly decreased for both donors due to treatment with pulsatile hydrostatic pressure. HSP70 was increased just in one of the donors. The list of proteins and their coordinate reference are reported in Table S1 and Fig. S2, respectively.

membrane potential) to green (low membrane potential) signal and are normalized to control samples. In Fig. 9(a) and (a'), FCCP corresponds to samples with depolarized mitochondrial membranes, serving as a control. None of the pressure modalities caused any statistical change in the mitochondrial membrane potential for either cell type, indicating that mitochondria remained intact after treatment.

Mechanical stimuli were reported to induce transcriptional activation of epithelial and endothelial cells via the activation of Piezo1 and subsequent signal transduction via Notch [40]. To study the potential activation of this pathway the expression of the two Notch1 target genes, *HES1* and *HEY1* were determined. Fig. 9(b, c) and (b', c') shows the mRNA expression of *HES1* and *HEY*1 for HaCaT and HUVEC, respectively. Our measurements show no statistical up/down-regulation of the targeted genes for either cell type or pressure modality.

4. Discussion

Mechanical stresses are intrinsically involved in nozzle-based bioprinting methods such as extrusion and inkjet bioprinting. Each of the individual mechanical stresses, shear stress or hydrostatic pressure, can potentially affect specific cellular responses. To carefully distinguish biological responses to bioprinting-associated hydrostatic pressure and to shear stress, a custom-made pressure setup was used by which we were able to impose hydrostatic pressure on cell suspensions. Cells were suspended in their medium and not in any type of hydrogel in order to exclude cell-hydrogel interactions. Two different modalities were considered: a) constant hydrostatic pressure resembling inkjet bioprinting using a mechanical microvalve, and b) pulsatile hydrostatic pressure resembling the extrusion-based method.

To date, it has been argued that hydrostatic pressure at the levels

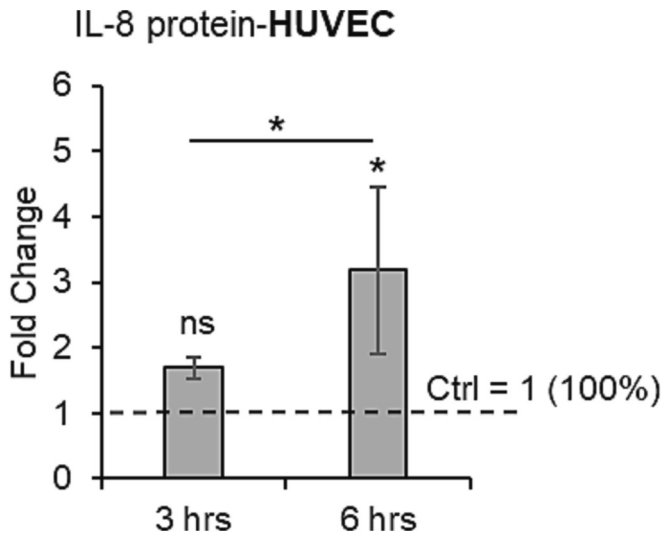

Fig. 8. IL-8 protein quantification. The measurement of IL-8 protein released by primary HUVECs showed a significant increase of this protein only 6 h after treatment with pulsatile hydrostatic pressure. Data are normalized to the values corresponding to the control sample (corresponding to the value = 1) and presented as fold change. The statistical analysis was performed on raw data (n = 3 and *p < 0.05).

involved in bioprinting, i.e., 1 to 5 bars, has only negligible effects on the viability of most cell types such as chondrocytes [41], Schwann, and 3T3 cells [5]. Instead, cell damage resulted mainly from too high shear and extensional stresses involved in nozzle-based bioprinting [7,8]. Indeed, our viability analysis (Fig. 2(a) and (b)) confirmed those findings for constant and pulsatile modalities of 1 bar gauge pressure imposed on HaCaT cells and primary HUVEC. Köpf et al. [42] showed that when printing at relatively high upstream pressure (3 bars) high level of cell death affects the network formation of endothelial cells. Therefore, the maintenance of an optimal cell survival rate throughout the bioprinting process is a primary requirement for biofabrication techniques. This was an additional reason for choosing 1.0 bar gage pressure as a reference in this work.

Physiologically relevant post-printing behavior of cells and the subsequent maturation of the printed structure are among the objectives of bioprinting. In order to address this concern, HaCaT and HUVEC were inspected for their cytoskeletal components to look for possible structural disruptions due to treatment with hydrostatic pressure (Figs. 2-4). We selected some of the cell-cell and cell-substrate contacts and their associated intermediate filament and actin networks since epithelial and endothelial cells rely on these to form a confluent monolayer able to serve as a physical barrier. Another reason for the selection was based on the debate among several groups about whether there is an effect of hydrostatic pressure on cell morphology and cytoskeletal structures [13,15,43]. Unfortunately, our results are not readily comparable to those of other groups for two main reasons: firstly, in our bioprinting process, the hydrostatic pressure is imposed on cells in suspension and the subsequent cell culturing is performed in ambient pressure while other groups have studied the effects of hydrostatic pressure on seeded cells in a period of hours to some days; and secondly, others have considered hydrostatic pressure in the range of 80–160 mmHg (0.11–0.22 bar), which is lower than what is usually used in the bioprinting process. Overall, we were not able to capture any cytoskeletal differences between treated and control samples, indicating that bioprinting-associated hydrostatic pressure in either pulsatile or constant modality does not affect the cellular structure and morphology or the ability of HaCaT and HUVEC to form a confluent monolayer. Here, our focus was on the structural evaluation of the cell cytoskeleton. Moreover, only a limited number of cell cytoskeletal components were considered in this work. In this regard, additional quantification of cell cytoskeletal components is of interest since they are involved in the regulation of various cellular behavior.

Recently, bioprinting of multicellular in vitro tissue models for drug

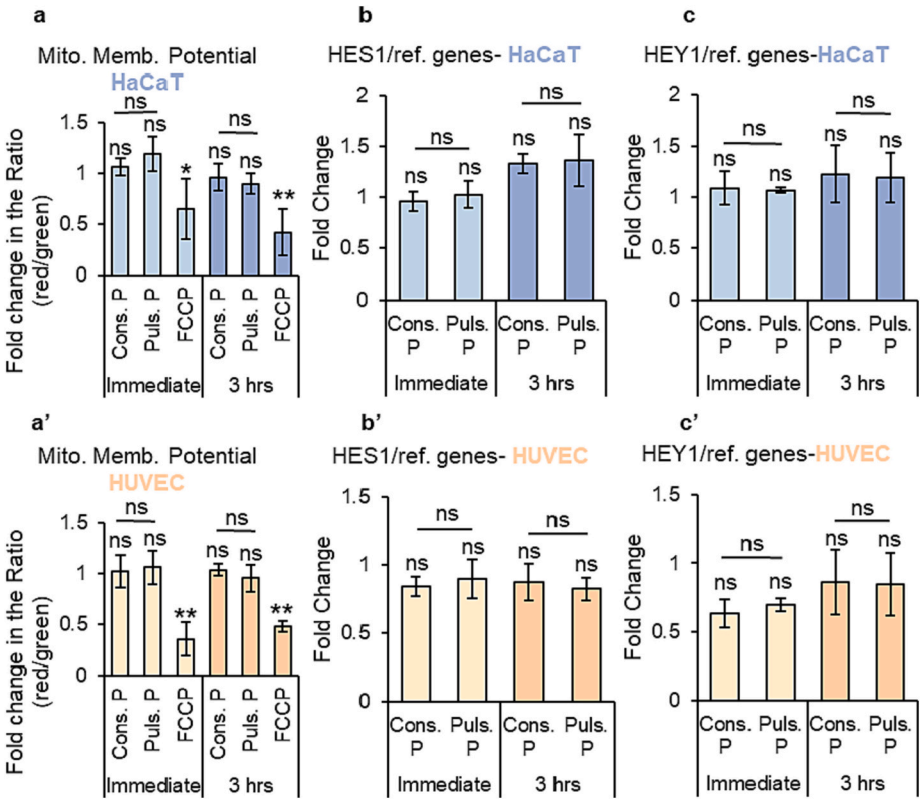

Fig. 9. Mitochondria and Piezo1 activity. There is no significant change in mitochondrial membrane potential due to treatment with hydrostatic pressure in either HaCaT cell line (a) or HUVEC (a'). The measurement was done using the cationic dye JC1 and the result is represented as the ratio of red (high membrane potentials) to green (low membrane potential) signal; FCCP corresponds to the samples with depolarized mitochondrial membrane, serving as a negative control with significant lower mitochondrial potential. The expression level of *HES1* for HaCaT cell line (b) and HUVEC (b') determined by qPCR reveal no significant over/under expression of this gene. The expression level of *HEY1* for HaCaT cell line (c) and HUVEC (c') determined by qPCR also reveals no significant over/under expression of this gene. All data are normalized to values corresponding to Ctrl sample (corresponding to the value = 1) and presented as fold change. The statistical analysis was performed on raw data (n ≥ 3 and *p < 0.05).

screening and disease modeling [44–46] as well as intra-operative bioprinting [47,48] have gained particular attention. In such applications, complex cellular responses such as inflammation, one of the complex biological responses of tissue that has both physiological and pathological roots [49], are expected. An example of the significance of the inflammatory response in post-surgical intervention can be found in the study of Shine et al. [50], where they showed that modulating the inflammatory response using a bioprinted polymer scaffold able to sequester excess pro-inflammatory cytokines from the site of injury helps to minimize postsurgical complications. Moreover, it is established that mechanical stress can potentially activate pro-inflammatory cytokines [16,51–53]. Accordingly, we hypothesized that bioprinting-associated hydrostatic pressure itself triggers the inflammatory response of processed cells. Based on our results, we can confirm that the pulsatile modality of hydrostatic pressure triggers the pro-inflammatory response of endothelial cells by increasing the mRNA level of *IL-8* (Fig. 6 (b')) and decreasing the expression of antithrombotic *THBD* (Fig. 6(c')). Treatment of primary HUVEC with pulsatile hydrostatic pressure increased the release of IL-8 protein 6 h after treatment. Additionally, it increased the intracellular ATP level of both HaCaT and HUVEC (Fig. 6 (a) and (a')). Since the pulsatile hydrostatic pressure modality resembles the conditions in the reservoir of a micro-extrusion bioprinter, we conclude that micro-extrusion bioprinting is powerful in triggering the pro-inflammatory response while inkjet bioprinting is not. Moreover, different parameters potentially influence this response such as the total time of treatment, the frequency and amplitude of hydrostatic pressure. An example of time-dependent inflammatory response to pulsatile hydrostatic pressure can be found in the study of Solis et al. [16].

In homeostasis, the levels of ATP and mitochondria membrane potential in a cell are kept relatively stable. Sustained changes can lead to unwanted loss of cell viability and be a cause of various pathologies [54]. In our results, the intracellular ATP returned to its baseline level 3 h after treatment. We also evaluated the mitochondrial membrane potential of the cells subjected to hydrostatic pressure. No significant change was found (Fig. 9(a) and (a')) in either of the pressure modalities or in either of the cell types. Together, these results indicate that even if the pulsatile modality of hydrostatic pressure increases the initial level of ATP, the effect is not harmful to the cell types studied here. This finding is potentially generalizable to the other cell types but it still might play a signaling role. ATP can be released by activation of a mechanosensitive ion-channel called Piezo1 [55,56]. For example, in urothelial cells, activation of Piezo1 ion-channels increases the level of cytosolic Ca^{2+}, leading to potential ATP release and signal [56]. In the case of Piezo1 activity, Notch1 target genes should be activated [40]. We analyzed the possibility of Piezo1 activation due to treatment with hydrostatic pressure considering its downstream events, i.e., expression of *HES1* and *HEY1*. The qPCR results did not confirm any significant change in the expression of *HES1* and *HEY1*. This finding is further supported by the fact that the cell membrane was not stretched by hydrostatic pressure, i.e., the cellular size did not change following treatment with pressure (Fig. 2(a) and (c)), leading to the conclusion that the possibility of Piezo1 involvement in the observed increased ATP production is low but not impossible. Further investigation is required in this context.

5. Conclusion

In this study, it has been demonstrated that treatment with pulsatile hydrostatic pressure can affect the inflammatory response of endothelial cells. This response did not occur at non-pulsating, i.e., constant hydrostatic pressure load, and was cell-type-dependent. At this level, it is hard to decide whether the microvalve inkjet or microextrusion technique is superior because the inflammatory response has both a physiologic and pathologic origin. Instead, the findings in this work identify characteristics of each bioprinting technique. One may note that the immediate interaction of the printed cells with native tissue and the immune system in vivo might potentially trigger a cascade of events. Therefore, our findings are more relevant for novel intra-operative, multicellular bioprinting approaches and for finding the proper bioprinting method for specific bioprinting scenarios and applications.

Supplementary data to this article can be found online at https://doi.org/10.1016/j.bioadv.2023.213329.

Funding

This work was supported by the Deutsche Forschungsgemeinschaft (DFG, grant number 363055819/GRK2415).

Author statement

Primary HUVEC were isolated from umbilical cords provided by the Department of Gynecology and Perinatal Medicine (RWTH Aachen University Hospital) as approved by the local ethics committee of the Faculty of Medicine at RWTH Aachen University (EK 424/19).

Declaration of competing interest

The authors have no conflicts of interest to state.

Data availability

Data will be made available on request.

Acknowledgment

We would like to thank Roswitha Davtalab and Michael Weber, Department of Dental Materials and Biomaterials Research, RWTH Aachen University Hospital, for their technical support.

References

[1] D. Kilian, T. Ahlfeld, A.R. Akkineni, A. Lode, M. Gelinsky, Three-dimensional bioprinting of volumetric tissues and organs, MRS Bull. 42 (8) (2017) 585–592.
[2] A. Shafiee, E. Ghadiri, H. Ramesh, C. Kengla, J. Kassis, P. Calvert, et al., Physics of bioprinting, Appl. Phys. Rev. [Internet] 6 (2) (2019), https://doi.org/10.1063/1.5087206. Available from:.
[3] J. Emmermacher, D. Spura, J. Cziommer, D. Kilian, T. Wollborn, U. Fritsching, et al., Engineering considerations on extrusion-based bioprinting: interactions of material behavior, mechanical forces and cells in the printing needle, Biofabrication [Internet] 12 (2) (2020) 25022, https://doi.org/10.1088/1758-5090/ab7553. Available from:.
[4] R. Chang, J. Nam, W. Sun, Effects of dispensing pressure and nozzle diameter on cell survival from solid freeform fabrication-based direct cell writing, Tissue Eng. - Part A 14 (1) (2008) 41–48, https://doi.org/10.1089/ten.a.2007.0004.
[5] M. Li, X. Tian, N. Zhu, D.J. Schreyer, X. Chen, Modeling process-induced cell damage in the biodispensing process, Tissue Eng. - Part CMethods 16 (3) (2010).
[6] Y.B. Bae, H.K. Jang, T.H. Shin, G. Phukan, T.T. Tran, G. Lee, et al., Microfluidic assessment of mechanical cell damage by extensional stress, Available from: Lab Chip [Internet] 16 (1) (2016) 96–103 www.rsc.org/loc.
[7] L. Ning, N. Betancourt, D.J. Schreyer, X. Chen, Characterization of cell damage and proliferative ability during and after bioprinting, ACS Biomater. Sci. Eng. 4 (11) (2018) 3906–3918.
[8] A. Blaeser, D.F. Duarte Campos, U. Puster, W. Richtering, M.M. Stevens, H. Fischer, Controlling shear stress in 3D bioprinting is a key factor to balance printing resolution and stem cell integrity, Adv. Healthc. Mater. 5 (3) (2016) 326–333.
[9] B. Frey, S. Franz, A. Sheriff, A. Korn, G. Bluemelhuber, U.S. Gaipl, et al., Hydrostatic pressure induced death of mammalian cells engages pathways related to apoptosis or necrosis, Cell Mol. Biol. 50 (4) (2004) 459–467.
[10] A.J. Steward, S.D. Thorpe, T. Vinardell, C.T. Buckley, D.R. Wagner, D.J. Kelly, Cell-matrix interactions regulate mesenchymal stem cell response to hydrostatic pressure, Acta Biomater. [Internet] 8 (6) (2012) 2153–2159, https://doi.org/10.1016/j.actbio.2012.03.016. Available from:.
[11] K. Maki, M.M. Nava, C. Villeneuve, M. Chang, K.S. Furukawa, T. Ushida, et al., Hydrostatic pressure prevents chondrocyte differentiation through heterochromatin remodeling, J. Cell Sci. 134 (2) (2021).
[12] A. Agar, S.S. Yip, M.A. Hill, M.T. Coroneo, Pressure related apoptosis in neuronal cell lines, J. Neurosci. Res. 60 (4) (2000) 495–503.
[13] T. Ohashi, Y. Sugaya, N. Sakamoto, M. Sato, Hydrostatic pressure influences morphology and expression of VE-cadherin of vascular endothelial cells, J. Biomech. 40 (11) (2007) 2399–2405.

[14] L. Tök, M. Nazirolu, A.C. Uuz, Ö. Tök, Elevated hydrostatic pressures induce apoptosis and oxidative stress through mitochondrial membrane depolarization in PC12 neuronal cells: a cell culture model of glaucoma, J. Recept. Signal Transduct. 34 (5) (2014) 410–416.
[15] E. Tworkoski, M.R. Glucksberg, M. Johnson, The effect of the rate of hydrostatic pressure depressurization on cells in culture, PLoS One [Internet] 13 (1) (2018) 1–21, https://doi.org/10.1371/journal.pone.0189890. Available from:.
[16] A.G. Solis, P. Bielecki, H.R. Steach, L. Sharma, C.C.D. Harman, S. Yun, et al., Mechanosensation of cyclical force by PIEZO1 is essential for innate immunity, Nature 573 (7772) (2019) 69–74.
[17] D. Ke, S.V. Murphy, Current challenges of bioprinted tissues toward clinical translation, Tissue Eng. - Part B Rev. 25 (1) (2019) 1–13.
[18] T.J. Hinton, A. Lee, A.W. Feinberg, 3D bioprinting from the micrometer to millimeter length scales: size does matter, Curr. Opin. Biomed. Eng. [Internet] 1 (2017) 31–37, https://doi.org/10.1016/j.cobme.2017.02.004. Available from:.
[19] N. Noor, A. Shapira, R. Edri, I. Gal, L. Wertheim, T. Dvir, 3D printing of personalized thick and perfusable cardiac patches and hearts, Adv. Sci. 6 (11) (2019).
[20] I. Matai, G. Kaur, A. Seyedsalehi, A. McClinton, C.T. Laurencin, Progress in 3D bioprinting technology for tissue/organ regenerative engineering, Biomaterials 226 (October 2019) (2020).
[21] H. Ravanbakhsh, V. Karamzadeh, G. Bao, L. Mongeau, D. Juncker, Y.S. Zhang, Emerging technologies in multi-material bioprinting, Adv. Mater. 33 (49) (2021).
[22] J. Schöneberg, F. De Lorenzi, B. Theek, A. Blaeser, D. Rommel, A.J.C. Kuehne, et al., Engineering biofunctional in vitro vessel models using a multilayer bioprinting technique, Sci. Rep. 8 (1) (2018) 1–13.
[23] N. Paxton, W. Smolan, T. Böck, F. Melchels, J. Groll, T. Jungst, Proposal to assess printability of bioinks for extrusion-based bioprinting and evaluation of rheological properties governing bioprintability [cited 2020 Aug 4]Available from, Biofabrication [Internet] 9 (4) (2017), https://doi.org/10.1088/1758-5090/aa8dd8.
[24] P. Boukamp, R.T. Petrussevska, D. Breitkreutz, J. Hornung, A. Markham, N. E. Fusenig, Normal keratinization in a spontaneously immortalized aneuploid human keratinocyte cell line, Available from, J. Cell Biol. [Internet] 106 (3) (1988 Mar) 761–771, http://www.ncbi.nlm.nih.gov/pubmed/2450098.
[25] K. Weißenbruch, J. Grewe, M. Hippler, M. Fladung, M. Tremmel, K. Stricker, et al., Distinct roles of nonmuscle myosin ii isoforms for establishing tension and elasticity during cell morphodynamics, elife 10 (2021) 1–35.
[26] M. Vicente-Manzanares, X. Ma, R.S. Adelstein, A.R. Horwitz, Non-muscle myosin II takes centre stage in cell adhesion and migration, Nat. Rev. Mol. Cell Biol. 10 (11) (2009) 778–790.
[27] C.E. Turner, Paxillin interactions, J. Cell Sci. 113 (23) (2000) 4139–4140.
[28] M.D. Schaller, Paxillin: a focal adhesion-associated adaptor protein, Oncogene 20 (44 REV. ISS. 5) (2001) 6459–6472.
[29] G. Cooper, Cell-cell interactions [Internet], Available from:, in: The Cell: A Molecular Approach, 2nd editio, Sinauer Associates, Sunderland (MA), 2000 https://www.ncbi.nlm.nih.gov/books/NBK9851/.
[30] D. Vestweber, VE-cadherin: the major endothelial adhesion molecule controlling cellular junctions and blood vessel formation, Available from, Arterioscler. Thromb. Vasc. Biol. [Internet] 28 (2) (2008 Feb) 223–232, http://www.ncbi.nlm.nih.gov/pubmed/18162609.
[31] J.M. Dave, K.J. Bayless, Vimentin as an integral regulator of cell adhesion and endothelial sprouting, Available from, Microcirculation [Internet] 21 (4) (2014 May) 333–344, http://www.ncbi.nlm.nih.gov/pubmed/24387004.
[32] J. Dunn, M.H. Grider, Physiology, Adenosine Triphosphate [Internet], Available from:, StatPearls, 2022 http://www.ncbi.nlm.nih.gov/pubmed/31985968.
[33] B. Wolff, A.R. Burns, J. Middleton, A. Rot, Endothelial cell "memory" of inflammatory stimulation: human venular endothelial cells store interleukin 8 in Weibel-Palade bodies, Available from, J. Exp. Med. [Internet] 188 (9) (1998 Nov 2) 1757–1762, http://www.ncbi.nlm.nih.gov/pubmed/9802987.
[34] Y. Matsuo, N. Ochi, H. Sawai, A. Yasuda, H. Takahashi, H. Funahashi, et al., CXCL8/IL-8 and CXCL12/SDF-lα co-operatively promote invasiveness and angiogenesis in pancreatic cancer, Available from, Int. J. Cancer [Internet] 124 (4) (2009 Feb 15) 853–861, http://www.ncbi.nlm.nih.gov/pubmed/19035451.
[35] J. Wang, Y. Wang, S. Wang, J. Cai, J. Shi, X. Sui, et al., Bone marrow-derived mesenchymal stem cell-secreted IL-8 promotes the angiogenesis and growth of colorectal cancer, Available from, Oncotarget [Internet] 6 (40) (2015 Dec 15) 42825–42837, http://www.ncbi.nlm.nih.gov/pubmed/26517517.
[36] T. Ikezoe, J. Yang, C. Nishioka, G. Honda, M. Furihata, A. Yokoyama, Thrombomodulin protects endothelial cells from a calcineurin inhibitor-induced cytotoxicity by upregulation of extracellular signal-regulated kinase/myeloid leukemia cell-1 signaling, Available from, Arterioscler. Thromb. Vasc. Biol. [Internet] 32 (9) (2012 Sep) 2259–2270, https://www.ahajournals.org/doi/10.1161/ATVBAHA.112.251157.
[37] S. Navarro, P. Medina, E. Bonet, J. Corral, V. Martínez-Sales, L. Martos, et al., Association of the thrombomodulin gene c.1418C>T polymorphism with thrombomodulin levels and with venous thrombosis risk, Arterioscler. Thromb. Vasc. Biol. [Internet] 33 (6) (2013 Jun) 1435–1440. Available from: https://www.ahajournals.org/doi/10.1161/ATVBAHA.113.301360.
[38] S. Carsten, J. Helle, Q. Feng, M.J. Aebersold, A. Vahid, A. Sirianni, et al., Mechanical force induces mitochondrial fission, Elife (2017) 1–26.
[39] Q. Feng, S.S. Lee, B. Kornmann, A toolbox for organelle mechanobiology research-current needs and challenges, Micromachines 10 (8) (2019) 1–13.
[40] V. Caolo, M. Debant, N. Endesh, T.S. Futers, L. Lichtenstein, F. Bartoli, et al., Shear stress activates adam10 sheddase to regulate notch1 via the piezo1 force sensor in endothelial cells, Available from, Elife [Internet] 9 (2020) 1–18, http://www.ncbi.nlm.nih.gov/pubmed/32484440.
[41] J.J. Parkkinen, M.J. Lammi, R. Inkinen, M. Jortikka, M. Tammi, I. Virtanen, et al., Influence of short-term hydrostatic pressure on organization of stress fibers in cultured chondrocytes, Available from: J. Orthop. Res. [Internet] 13 (4) (1995 Jul) 495–502 http://doi.wiley.com/10.1002/jor.1100130404.
[42] M. Köpf, R. Nasehi, F. Kreimendahl, S. Jockenhoevel, H. Fischer, Bioprinting-associated shear stress and hydrostatic pressure affect the angiogenic potential of human umbilical vein endothelial cells, Int. J. Bioprinting [Internet] 8 (4) (2022 Aug 18). Available from: https://ijb.whioce.com/index.php/int-j-bioprinting/article/view/606.
[43] B.E. Sumpio, M.D. Widmann, J. Ricotta, M.A. Awolesi, M. Watase, Increased ambient pressure stimulates proliferation and morphologic changes in cultured endothelial cells, Available from, J. Cell Physiol. [Internet] 158 (1) (1994 Jan) 133–139, http://www.ncbi.nlm.nih.gov/pubmed/8263020.
[44] D.F. Duarte Campos, A. Bonnin Marquez, C. O'Seanain, H. Fischer, A. Blaeser, M. Vogt, et al., Exploring cancer cell behavior in vitro in three-dimensional multicellular bioprintable collagen-based hydrogels, Available from: Cancers (Basel) [Internet] 11 (2) (2019 Feb 5) http://www.ncbi.nlm.nih.gov/pubmed/30764492.
[45] S. Swaminathan, Q. Hamid, W. Sun, A.M. Clyne, Bioprinting of 3D breast epithelial spheroids for human cancer models, Biofabrication [Internet] 11 (2) (2019), 025003. Available from: http://www.ncbi.nlm.nih.gov/pubmed/30616234.
[46] J. Redmond, H. McCarthy, P. Buchanan, T.J. Levingstone, N.J. Dunne, Advances in biofabrication techniques for collagen-based 3D in vitro culture models for breast cancer research, Available from, Mater. Sci. Eng. C Mater. Biol. Appl. [Internet] 122 (2021 Mar), 111944, http://www.ncbi.nlm.nih.gov/pubmed/33641930.
[47] K.K. Moncal, R.S. Tigli Aydın, K.P. Godzik, T.M. Acri, D.N. Heo, E. Rizk, et al., Controlled co-delivery of pPDGF-B and pBMP-2 from intraoperatively bioprinted bone constructs improves the repair of calvarial defects in rats, Available from, Biomaterials [Internet] 281 (2022 Feb), 121333, http://www.ncbi.nlm.nih.gov/pubmed/34995904.
[48] K.K. Moncal, H. Gudapati, K.P. Godzik, D.N. Heo, Y. Kang, E. Rizk, et al., Intra-operative bioprinting of hard, soft, and hard/soft composite tissues for craniomaxillofacial reconstruction, Adv. Funct. Mater. [Internet] 31 (29) (2021 Jul 16). Available from: http://www.ncbi.nlm.nih.gov/pubmed/34421475.
[49] R. Medzhitov, Origin and physiological roles of inflammation, Available from, Nature [Internet] 454 (7203) (2008 Jul 1) 428–435, http://www.nature.com/articles/nature07201.
[50] C.S. Shin, F.J. Cabrera, R. Lee, J. Kim, R. Ammassam Veettil, M. Zaheer, et al., 3D-bioprinted inflammation modulating polymer scaffolds for soft tissue repair, Adv. Mater. [Internet] 33 (4) (2021 Jan), e2003778. Available from: http://www.ncbi.nlm.nih.gov/pubmed/33325594.
[51] G. Radley, S. Ali, I.L. Pieper, C.A. Thornton, Mechanical shear stress and leukocyte phenotype and function: implications for ventricular assist device development and use, Available from, Int. J. Artif. Organs [Internet] 42 (3) (2019 Mar 26) 133–142, http://journals.sagepub.com/doi/10.1177/0391398818817326.
[52] S.-K. Lee, K.-S. Min, Y.-. Kim, G.-S. Jeong, S.-H. Lee, H.-J. Lee, et al., Mechanical stress activates proinflammatory cytokines and antioxidant defense enzymes in human dental pulp cells, J. Endod. [Internet] 34 (11) (2008 Nov) 1364–1369. Available from: https://linkinghub.elsevier.com/retrieve/pii/S0099239908007486.
[53] D.A. Chistiakov, A.N. Orekhov, Y.V. Bobryshev, Effects of shear stress on endothelial cells: go with the flow, Available from, Acta Physiol. [Internet] 219 (2) (2017 Feb) 382–408, https://onlinelibrary.wiley.com/doi/10.1111/apha.12725.
[54] L.D. Zorova, V.A. Popkov, E.Y. Plotnikov, D.N. Silachev, I.B. Pevzner, S. S. Jankauskas, et al., Mitochondrial membrane potential, Available from, Anal. Biochem. [Internet] 552 (2018) 50–59, http://www.ncbi.nlm.nih.gov/pubmed/28711444.
[55] B. Coste, J. Mathur, M. Schmidt, T.J. Earley, S. Ranade, M.J. Petrus, et al., Piezo1 and Piezo2 are essential components of distinct mechanically activated cation channels, Science [Internet] 330 (6000) (2010 Oct 1) 55–60. Available from: http://www.ncbi.nlm.nih.gov/pubmed/20813920.
[56] T. Miyamoto, T. Mochizuki, H. Nakagomi, S. Kira, M. Watanabe, Y. Takayama, et al., Functional role for Piezo1 in stretch-evoked Ca2+ influx and ATP release in urothelial cell cultures, Available from, J. Biol. Chem. [Internet] 289 (23) (2014 Jun 6) 16565–16575, http://www.ncbi.nlm.nih.gov/pubmed/24759099.